Constraining the minimal type-III seesaw model with naturalness, lepton flavor violation, and electroweak vacuum stability

Srubabati Goswami,[1,*] Vishnudath K. N.,[1,2,†] and Najimuddin Khan[3,‡]

[1]*Theoretical Physics Division, Physical Research Laboratory, Ahmedabad 380009, India*
[2]*Discipline of Physics, Indian Institute of Technology, Gandhinagar 382355, India*
[3]*Centre for High Energy Physics, Indian Institute of Science,*
C. V. Raman Avenue, Bangalore 560012, India

We study the minimal type-III seesaw model in which we extend the standard model by adding two $SU(2)_L$ triplet fermions with zero hypercharge to explain the origin of the nonzero neutrino masses. We show that the naturalness conditions and the limits from lepton flavor violating decays provide very stringent bounds on the model parameters along with the constraints from the stability/metastability of the electroweak vacuum. We perform a detailed analysis of the model parameter space including all the constraints for both normal as well as inverted hierarchies of the light neutrino masses. We find that most of the regions that are allowed by lepton flavor violating decays and naturalness fall in the stable/metastable region depending on the values of the standard model parameters.

I. INTRODUCTION

The discovery of the Higgs boson [1,2] at the Large Hadron Collider (LHC) has confirmed the mode of generation of the masses of the fundamental particles via the mechanism of electroweak (EW) symmetry breaking and has put the standard model (SM) on a solid foundation. However, despite its success in explaining most of the experimental data, the SM cannot address certain issues. One of the most important experimental observations that necessitates the extension of the SM is the phenomenon of neutrino oscillation. The solar, atmospheric, reactor, and accelerator neutrino oscillation experiments have shown that the three neutrino flavors mix among themselves, and they have very small but nonzero masses, unlike as predicted in the SM.

Among the various beyond the standard model scenarios that are proposed in the literature to explain the small neutrino masses, the most popular one is the seesaw mechanism. This is based on the assumption that the lepton number is violated at a very high energy scale by some heavier particles. The tree level exchange of these heavy particles generates the lepton number violating dimension-five Weinberg operator $\kappa LLHH$ [3]. This gives rise to small neutrino masses once the EW symmetry is broken. Here, L and H are the lepton and Higgs doublets, respectively, and κ is a proportionality constant with negative mass dimension and is inversely proportional to the energy scale at which the new physics enters. Depending on the nature of the heavy particles added for the ultraviolet completion, one can have three types of seesaw mechanisms. If the seesaw is generated by adding extra neutral fermionic singlets, it is called a type-I seesaw mechanism [4–7]. Similarly, a type-II seesaw mechanism is generated by adding a triplet scalar [8–11] to the SM, whereas the addition of fermionic triplets gives rise to the type-III seesaw mechanism [12]. It is known that in order to get a neutrino mass of the sub-eV scale, one has to take the new particles to be extremely heavy or else take the new couplings to be extremely small. This spoils the testability of the theory. However, there are various TeV scale extensions of the canonical scenarios proposed in the literature [13–17], which can be probed at the collider experiments (for recent reviews, see, for instance, [18,19]). In the case of type-I and type-III seesaw models, one can also have large Yukawa couplings and new fermions of masses in the TeV scale by choosing some particular textures of the neutrino Yukawa coupling matrix [20–22].

An important aspect to be considered while studying the seesaw models is the issue of naturalness. It is well known that the Higgs mass gets large corrections from the higher order loop diagrams due to its self-interaction as well as the couplings with gauge bosons and fermions. The theory is

*[*]sruba@prl.res.in
[†]vishnudath@prl.res.in
[‡]khanphysics.123@gmail.com

perceived unnatural if a severe fine-tuning between the quadratic radiative corrections and the bare mass is needed to bring down Higgs mass to the observed scale. It is well known that although the dimensional regularization can throw away the quadratic divergences, the presence of other dangerous logarithmic and finite contributions can cause a similar naturalness problem. In the case of seesaw models in which the new particles couple to the SM Higgs, this naturalness problem is enhanced [23–33]. Demanding the correction to the Higgs mass to be of the order of TeV can bring down the seesaw scale.

Another aspect of low-scale seesaw models which has received attention lately is the implications of such scenarios for the stability of the EW vacuum. It is to be noted that the observed value of the Higgs mass of 125.7 ± 0.3 GeV is quite intriguing from the viewpoint of the EW vacuum stability. The measured values of the SM parameters, especially the top mass M_t and strong coupling constant α_s, suggest that an extra deeper minima resides near the Planck scale, threatening the stability of the present EW vacuum [34,35], since this may tunnel into that true (deeper) vacuum. The decay probability has been calculated using the state-of-the-art next-to-next-to-leading-order corrections, and it suggests that the present EW vacuum is metastable at 3σ, which means that the decay time is greater than the age of the Universe. It is well known that the scalar couplings pull the vacuum towards stability, whereas the Yukawa couplings push it towards instability. Thus, in the case of seesaw models, the Yukawa couplings as well as the masses of the new fermions will also get bounded by the constraints from the stability/metastability of the EW vacuum [36–49]. In particular, in Ref. [50], the authors have discussed the implications of vacuum stability and gauge-Higgs unification in the context of the type-III seesaw model, and Ref. [45] has discussed the EW vacuum metastability in the context of type-I as well as type-III seesaw models. In Ref. [32], the authors have studied the implications of naturalness and vacuum stability in a minimal type-I seesaw model. Similarly, the naturalness and vacuum stability in the case of the type-II seesaw model have been studied in Ref. [31].

In this paper, we study the consequences of naturalness in the minimal type-III seesaw model, in which we extend the SM by adding two $SU(2)_L$ triplet fermions with zero hypercharge to explain the origin of the nonzero neutrino masses and mixing. To give mass to all three light active neutrinos, one needs three triplet fermions. Hence, in the minimal type-III seesaw model, the lightest active neutrino will be massless. We use the Casas-Ibarra (CI) parametrization for the neutrino Yukawa coupling matrix [51,52], and by choosing the two triplets to be degenerate, we have only three independent real parameters, namely, the mass of the triplet fermions and a complex angle in the CI parametrization. We study and constrain the bounds on these model parameters by demanding that the theory be

natural. In addition, we also study the bounds on the model from the EW vacuum metastability as well as lepton flavor violating (LFV) decays.

The rest of the paper is organized as follows: In Sec. II, we review the minimal type-III seesaw model and the parametrization used for our studies. In Sec. III, we discuss the implications of naturalness in the minimal type-III seesaw model, and in Sec. IV, we discuss the constraints from the LFV decays. After this, we discuss the effective Higgs potential in the presence of the extra fermion triplets and the renormalization group (RG) evolution of the different couplings and present a detailed discussion of the results. Finally, we summarize in Sec. VI.

II. THE MINIMAL TYPE-III SEESAW MODEL

We extend the standard model with two fermionic triplets Σ_{R_i}, $i = 1, 2$ having zero hypercharge, which can be represented as

$$\Sigma_R = \begin{bmatrix} \Sigma_R^0/\sqrt{2} & \Sigma_R^+ \\ \Sigma_R^- & -\Sigma_R^0/\sqrt{2} \end{bmatrix} \equiv \frac{\Sigma_R^i \sigma^i}{\sqrt{2}}, \qquad (2.1)$$

where $\Sigma_R^\pm = (\Sigma_R^1 \mp i\Sigma_R^2)/\sqrt{2}$. The parts of the Lagrangian that are relevant to neutrino mass generation are

$$-\mathcal{L}_\Sigma = \tilde{\Phi}^\dagger \bar{\Sigma}_R \sqrt{2} Y_\Sigma L + \frac{1}{2} \mathrm{Tr}[\bar{\Sigma}_R M \Sigma_R^c] + \mathrm{H.c.}, \qquad (2.2)$$

where the generation indices have been suppressed. In the above equation, $L = (\nu_l \, l^-)^T$ is the lepton doublet and $\tilde{\Phi} = i\sigma_2 \Phi^*$ (σ_2 is the second Pauli matrix). For simplicity, we consider the scenario in which the Majorana mass matrix M is proportional to the identity matrix so that the heavy fermions have degenerate masses denoted by M_Σ. Once the Higgs field Φ acquires a vacuum expectation value (VEV), the neutral fermion mass matrix can be written as

$$M_\nu = \begin{pmatrix} 0 & M_D^T \\ M_D & M \end{pmatrix}. \qquad (2.3)$$

Here, $M_D = Y_\Sigma v/\sqrt{2}$, where $v = 246$ GeV is the VEV of the SM Higgs. The given mass matrix can be diagonalized by a unitary matrix U_0 as

$$U_0^T M_\nu U_0 = M_\nu^{\mathrm{diag}} = \mathrm{diag}(m_1, m_2, m_3, M_\Sigma, M_\Sigma), \quad (2.4)$$

where M is the mass of the heavy triplet fermions. Note that the lightest neutrino is massless in this scenario. We can write the matrix U_0 as [53]

$$U_0 = W U_\nu \simeq \begin{pmatrix} (1 - \frac{1}{2}\epsilon)U & M_D^\dagger (M^{-1})^* U_R \\ -M^{-1} M_D U & (1 - \frac{1}{2}\epsilon')U_R \end{pmatrix}$$

$$\equiv \begin{pmatrix} U_L & T \\ S & U_H \end{pmatrix}. \tag{2.5}$$

Here, W brings the full 5×5 mass matrix to the block diagonal form, and U and U_R diagonalize the light and heavy neutrino mass matrices, respectively. In our case, U_R is a 2×2 identity matrix. U_L is the Pontecorvo-Maki-Nakagawa-Sakata (PMNS) mixing matrix with a small nonunitary correction. The nonunitarity is characterized by ϵ and ϵ' and is given by

$$\epsilon = TT^\dagger = M_D^\dagger (M^{-1})^* M^{-1} M_D,$$
$$\epsilon' = SS^\dagger = M^{-1} M_D M_D^\dagger (M^{-1})^*. \tag{2.6}$$

In the limit $M \gg M_D$, the light neutrino mass matrix can be written as

$$m_{\text{light}} = -M_D^T M^{-1} M_D. \tag{2.7}$$

We use the Casas-Ibarra parametrization [51,52] for the Yukawa coupling matrix Y_Σ, such that the constraints on the light neutrino mixing angles as well as the mass squared differences as predicted from the oscillation data are automatically satisfied. In this parametrization,

$$Y_\Sigma = \frac{\sqrt{2}}{v} \sqrt{D_\Sigma} R \sqrt{D_\nu} U^\dagger, \tag{2.8}$$

where $D_\Sigma = \text{diag}(M_\Sigma, M_\Sigma)$, $D_\nu = \text{diag}(m_1, m_2, m_3)$, and R is an arbitrary complex 2×3 orthogonal matrix which parametrizes the information that is lost in the decoupling of the triplet fermions. The light neutrino masses for the normal hierarchy (NH) and inverted hierarchy (IH) are given by

$$m_1 = 0, \quad m_2 = \sqrt{\Delta m_{\text{sol}}^2}, \quad m_3 = \sqrt{\Delta m_{\text{atm}}^2}(\text{NH})$$

$$m_1 = \sqrt{\Delta m_{\text{atm}}^2}, \quad m_2 = \sqrt{\Delta m_{\text{sol}}^2 + \Delta m_{\text{atm}}^2}, \quad m_3 = 0(\text{IH}). \tag{2.9}$$

We use the following parametrization of the PMNS matrix U,

$$U = \begin{pmatrix} c_{12}c_{13} & s_{12}c_{13} & s_{13}e^{-i\delta} \\ -c_{23}s_{12} - s_{23}s_{13}c_{12}e^{i\delta} & c_{23}c_{12} - s_{23}s_{13}s_{12}e^{i\delta} & s_{23}c_{13} \\ s_{23}s_{12} - c_{23}s_{13}c_{12}e^{i\delta} & -s_{23}c_{12} - c_{23}s_{13}s_{12}e^{i\delta} & c_{23}c_{13} \end{pmatrix} P, \tag{2.10}$$

where $c_{ij} = \cos\theta_{ij}$, $s_{ij} = \sin\theta_{ij}$, and the phase matrix $P = \text{diag}(e^{-i\alpha}, e^{+i\alpha}, 1)$ contains the Majorana phases.

In our numerical analysis, we have used the values of mass squared differences and mixing angles in the 3σ ranges as shown in Table I [54] and varied the phases δ and α between $-\pi$ to $+\pi$. It has been shown in Ref. [52] that the matrix R can be parametrized as

$$R = \begin{cases} \begin{pmatrix} 0 & \cos z & \zeta \sin z \\ 0 & -\sin z & \zeta \cos z \end{pmatrix} & (\text{NH}), \\ \begin{pmatrix} \cos z & \zeta \sin z & 0 \\ -\sin z & \zeta \cos z & 0 \end{pmatrix} & (\text{IH}), \end{cases} \tag{2.11}$$

where z is a complex parameter and $\zeta = \pm 1$. We fix the value of ζ to be $+1$ for our entire analysis, and this does not change any of our results. Thus, the only free parameters in the model are the mass of the triplet fermions M_Σ and the complex number z. z can take any value in the complex plane.

Note that in this model, the charged components of the triplet fermions mix with the SM charged leptons. This is governed by the Lagrangian [55]

$$L = -(\bar{l}_R \ \bar{\Psi}_R) \begin{pmatrix} m_l & 0 \\ \sqrt{2}M_D & M \end{pmatrix} \begin{pmatrix} l_L \\ \Psi_L \end{pmatrix} + \text{H.c.}, \tag{2.12}$$

where we have defined

$$\Psi = \Sigma_R^{+c} + \Sigma_R^-. \tag{2.13}$$

The charged fermion mass matrix given in the above equation can be diagonalized by a biunitary transformation.

Since the additional heavy triplet fermions have the $SU(2)$ gauge interactions, they can be produced and detected in the collider experiments through the process(es) $pp \to \Sigma^+ \Sigma^- \to mj + nl + \cancel{E}_T$ (m, n are integers). The collider study of extra triplet fermions was first explored in Ref. [56] in the context of an $SU(5)$ grand unified model.

TABLE I. The oscillation parameters in their 3σ range for both NH and IH as given by the global analysis of neutrino oscillation data with three light active neutrinos [54].

Parameter	NH	IH
$\Delta m_{21}^2 / 10^{-5}$ eV^2	$6.80 \to 8.02$	$6.80 \to 8.02$
$\Delta m_{3l}^2 / 10^{-3}$ eV^2	$+2.399 \to +93$	$-62 \to -2.369$
$\sin^2\theta_{12}$	$0.272 \to 0.346$	$0.272 \to 0.346$
$\sin^2\theta_{23}$	$0.418 \to 0.613$	$0.435 \to 0.616$
$\sin^2\theta_{13}$	$0.01981 \to 0.02436$	$0.02006 \to 0.02452$

Since then, a lot of work has been done on the phenomenology of the type-III seesaw model in the context of the LHC [57–64]. The experimental searches performed by the CMS and ATLAS Collaborations have put lower bounds on the triplet masses. CMS [65] has set a lower limit of 430 GeV on the triplet mass with the data from the $\sqrt{s} = 13$ TeV run, whereas depending on the various scenarios studied, the ATLAS results rule out masses in the range below 325–540 GeV [66]. Recently, the authors of Ref. [67] have studied the phenomenology of the type-III seesaw model in the context of high energy e^+e^- colliders.

III. NATURALNESS

One of the problems associated with the high-scale seesaw models is that the associated heavy particles give very large corrections to the Higgs mass making the theory unnatural. Here, we shall see the implications of naturalness in the context of the type-III seesaw scenario. The tree level SM Higgs potential is given by

$$V = -\mu^2(\Phi^\dagger\Phi) + \lambda(\Phi^\dagger\Phi)^2, \qquad (3.1)$$

where

$$\Phi = \frac{1}{\sqrt{2}}\begin{pmatrix} G^+ \\ v + h + iG^0 \end{pmatrix}. \qquad (3.2)$$

Here, the VEV $v = 246$ GeV, and this will give the physical Higgs particle with tree level mass as $m_h^2 = 2\lambda v^2$. For the naturalness of the Higgs mass, the heavy right-handed neutrino loop corrections to the mass parameter μ should be smaller than $O(\text{TeV}^2)$. In the $\overline{\text{MS}}$ scheme, the correction is given by

$$\delta\mu^2 \approx \frac{3}{4\pi^2}\text{Tr}[Y_\Sigma^\dagger D_\Sigma^2 Y_\Sigma]. \qquad (3.3)$$

Note that we have taken the quantity $(\ln[\frac{M_\Sigma}{\mu_R}] - \frac{1}{2})$ to be unity (where μ_R is the renormalization scale). Now, using the parametrization in Eq. (2.8), we get

$$\begin{aligned} \delta\mu^2 &\approx \frac{3}{4\pi^2}\frac{2}{v^2}\text{Tr}[D_\nu R^\dagger D_\Sigma^3 R] \\ &= \frac{3M_\Sigma^3}{2\pi^2 v^2}\cosh(2\text{Im}[z]) \\ &\times \begin{cases} \sqrt{\Delta m_{\text{sol}}^2} + \sqrt{\Delta m_{atm}^2} & \text{(NH)}, \\ \sqrt{\Delta m_{atm}^2} + \sqrt{\Delta m_{\text{sol}}^2 + \Delta m_{atm}^2} & \text{(IH)}. \end{cases} \end{aligned} \qquad (3.4)$$

From the above expressions, we can see that the only unknown parameters are M_Σ and $\text{Im}[z]$.

In Fig. 1, we have presented the naturalness contours in the $\text{Im}[z]$-M_Σ plane for both NH and IH. In the shaded regions, $\delta\mu^2$ is demanded to be less than $p\%$ of 1 TeV^2 where $p = 500, 100, 50, 20, 10, 5, 1$ (from top to bottom). The unshaded regions are disfavored by naturalness. From these plots, we can see that higher the mass of the triplet, the smaller the allowed values of the $\text{Im}[z]$. For instance, demanding $\delta\mu^2 < (1 \text{ TeV})^2$ implies that $M_\Sigma \leq 1.84 \times 10^7$ GeV for $\text{Im}[z] = 0$ and $M_\Sigma \leq 3 \times 10^5$ GeV for $\text{Im}[z] = 6$. These bounds become even more stringent as we demand $\delta\mu^2$ to be smaller as can be seen from the plots. Also, from Eq. (3.4), we can see that the $\delta\mu^2$ values for NH and IH differ roughly by a factor of one-half ($\Delta m_{atm}^2 \gg \Delta m_{\text{sol}}^2$). This effect can be seen from the fact that for a given value of $\text{Im}(z)$, the maximum allowed value of M_Σ for NH is slightly higher than that for IH.

(a) Naturalness contour for NH
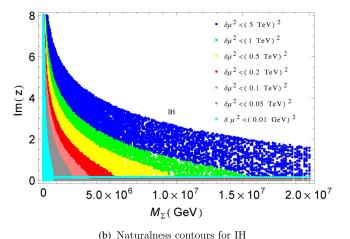

(b) Naturalness contours for IH

FIG. 1. Naturalness contours in the $\text{Im}[z]$-M_Σ plane. Plot (a) is for NH, and plot (b) is for IH. In the shaded regions, $\delta\mu^2$ is less than $p\%$ of 1 TeV^2 where $p = 500, 100, 50, 20, 10, 5, 1$ (from top to bottom). The unshaded regions are disfavored by naturalness.

IV. CONSTRAINTS FROM THE LEPTON FLAVOR VIOLATION

The decay widths and the branching ratios for the various lepton flavor violating decays in the context of the type-III seesaw model have been worked out in Ref. [55]. This model can have the decays $\mu \to e\gamma$ and $\tau \to l\gamma$ at the one-loop level and $\mu \to 3e$ as well as the $\tau \to 3l$ processes at the tree level due to the charged lepton mixing. However, among all the LFV decays, the most stringent bound is the one coming from the μ to e conversion in the nuclei. The $\mu \to e$ conversion rate to the total nucleon muon capture rate ratio ($R^{\mu \to e}$) puts a bound on $\epsilon_{e\mu}$. For the $^{48}_{22}$Ti nuclei, we have [68]

$$R^{\mu \to e} < 4.3 \times 10^{-12}, \tag{4.1}$$

and the bound from this is the most stringent among all the LFV bounds in the triplet fermion model and is given as [55]

$$\epsilon_{e\mu} < 1.7 \times 10^{-7}. \tag{4.2}$$

We present the constraints on z and M_Σ from this bound in Fig. 2 for both the NH and IH. The regions above the blue dotted line are disallowed by the LFV bounds, whereas the regions to the right of the purple, magenta, and brown solid lines are disallowed by the naturalness bounds depending on the naturalness condition used. We can clearly see that the naturalness bounds restrict larger values of M_Σ, whereas the LFV bound constrains the larger values of Im(z) corresponding to the smaller values of M_Σ. The unshaded region is the one that is allowed by both LFV as well as the naturalness bounds. One can notice from these plots that for both the NH and IH, the maximum allowed value of Im(z) is ~ 10, which corresponds to a

triplet mass of $\sim 10^4$ GeV. In generating these plots, we have varied the light neutrino mass squared differences and mixing angles in their 3σ ranges, the Dirac and Majorana phases are varied in the range $0 - \pi$, and we have presented the most stringent bounds.
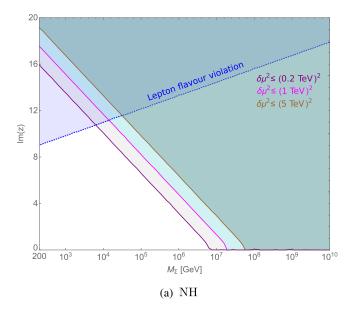
V. VACUUM STABILITY

In this section, we discuss how the stability of the EW vacuum is modified in the presence of the extra fermionic triplets if we assume that there is no other new physics up to the Planck scale. It is well known that if we have extra fermions, they tend to destabilize the EW vacuum. We aim to quantify this effect and obtain constraints in the context of the model outlined. In the following, we discuss the theoretical background and tools needed in the stability analysis of the EW vacuum up to the Planck scale such as the Higgs effective potential which determines the instability, metastability, stability, and perturbative-unitary scales, the proper matching conditions which give the initial values of the model parameters at the EW scale, the RGEs delineating the running of the couplings, and the other parameters from the EW scale up to the Planck scale M_{Pl}.

The SM one-loop effective Higgs potential in the $\overline{\text{MS}}$ scheme and the Landau gauge can be written as

$$V_1^{SM}(h) = \sum_{i=1}^{5} \frac{n_i}{64\pi^2} M_i^4(h) \left[\ln \frac{M_i^2(h)}{\mu^2(t)} - c_i \right], \tag{5.1}$$

where the index i is summed over all SM particles, $M_i^2(h) = \kappa_i(t)h^2(t) - \kappa_i'(t)$ and $c_{h,G,f} = 3/2$, $c_{W,Z} = 5/6$ [69–73]. n_i is the number of degrees of freedom of the particle fields. The values of n_i, κ_i, and κ_i' are given in
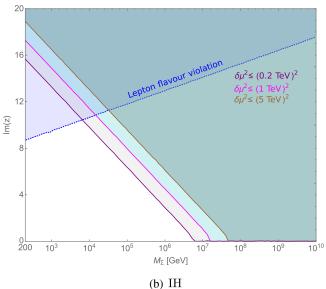

FIG. 2. Bounds on z from lepton flavor violation (blue dotted line) and naturalness (purple, magenta, and brown solid lines). Plot (a) is for NH, and plot (b) is for IH. The unshaded region is allowed by both LFV as well as naturalness bounds.

Eq. (4) in [69]. The above contribution comes with a positive sign for the gauge and scalar bosons, whereas it is negative for the fermion fields. The running energy scale μ is related to a dimensionless parameter t as $\mu(t) = M_Z \exp(t)$.

Following the method outlined in [38,49,74], the additional contribution to the one-loop effective potential from the fermionic triplet is given as

$$V_1^\Sigma(h) = -\frac{3(M_D^\dagger(h)M_D(h))_{ii}^2}{32\pi^2}\left[\ln\frac{(M_D^\dagger(h)M_D(h))_{ii}}{\mu^2(t)} - \frac{3}{2}\right]$$
$$-\frac{3(M_D(h)M_D^\dagger(h))_{jj}^2}{32\pi^2}\left[\ln\frac{(M_D(h)M_D^\dagger(h))_{jj}}{\mu^2(t)} - \frac{3}{2}\right],$$
(5.2)

where $M_D(h) = \frac{Y_\Sigma}{\sqrt{2}}h$, and i, j run over the three light neutrinos and the two triplet fermions, respectively. In this analysis, we use the two-loop contributions to the effective potential for the SM particles, whereas the contribution due to the extra fermion triplet is considered up to one loop only. For high field value $h(t) \gg v$, the effective potential can be approximated as $V_{\rm eff}^{SM+\Sigma} = \lambda_{\rm eff}(h)\frac{h^4}{4}$. The one- and two-loop SM expressions for $\lambda_{\rm eff}(h)$ can be found in Ref. [35]. The contribution due to the extra fermionic triplet is obtained as

$$\lambda_{\rm eff}^\Sigma(h) = -\frac{3e^{4\Gamma(h)}}{32\pi^2}\left((Y_\Sigma^\dagger Y_\Sigma)_{ii}^2\left(\ln\frac{(Y_\Sigma^\dagger Y_\Sigma)_{ii}}{2} - \frac{3}{2}\right)\right.$$
$$\left. + (Y_\Sigma Y_\Sigma^\dagger)_{jj}^2\left(\ln\frac{(Y_\Sigma Y_\Sigma^\dagger)_{jj}}{2} - \frac{3}{2}\right)\right),$$
(5.3)

where the factor $\Gamma(h) = \int_{M_t}^h \gamma(\mu)d\ln\mu$ indicates the wave function renormalization of the Higgs field. Here, $\gamma(\mu)$ is the anomalous dimension of the Higgs [69–73], the contribution to which from the fermion triplet at one loop is $\frac{3}{2}{\rm Tr}(Y_\Sigma Y_\Sigma^\dagger)$. We also assume that $\mu = h$. In this choice, all the running coupling constants ensure faster convergence of the perturbation series of the potential [75].

We compute the RG evolution of all the couplings to analyze the Higgs potential up to the Planck scale. We first calculate all the SM couplings at the top mass scale M_t, taking care of the threshold corrections [76–79]. We use one-loop RGEs to calculate $SU(2)$ and $U(1)$ gauge couplings $g_2(M_t)$ and $g_1(M_t)$.[1] For the $SU(3)$ gauge coupling $g_3(M_t)$, we use three-loop RGEs considering contributions from the five quarks and the effect of the sixth; i.e., the top quark has been taken using an effective field theory approach. We also include the leading term in the four-loop RGE for α_s. The mismatch between the top

---

[1]Our result will not change significantly even if we use the two-loop RGEs for g_1 and g_2.

pole mass and the $\overline{\rm MS}$ renormalized coupling has been taken care of by using the threshold correction $y_t(M_t) = \frac{\sqrt{2}M_t}{v}(1 + \delta_t(M_t))$, where $\delta_t(M_t)$ is the matching correction for y_t at the top pole mass. We use $\lambda(M_t) = \frac{M_H^2}{2v^2}(1 + \delta_H(M_t))$ for the Higgs quartic coupling λ. To calculate this at the scale M_t, we have included the QCD corrections up to three loops [80], electroweak corrections up to one loop [81,82], and $O(\alpha\alpha_s)$ corrections to the matching of top Yukawa and top pole mass [77,83]. We have reproduced the SM couplings at M_t as in Refs. [35,79] by using these threshold corrections. We evolve them up to the heavy fermionic mass scale using the SM RGEs [84–87]. The extra contributions due to the femionic triplets are included after the threshold heavy fermionic mass scale [88]. Then we evolve all the couplings up to the Planck scale to find the position and depth of the new minima at the high scale.

It is well known that if the EW vacuum of the Higgs potential is not the global minimum, then a quantum tunneling to the true vacuum may occur. This happens because the RG running can make the quartic coupling λ negative at a high energy scale. However, this does not pose a threat to the theory if the decay time is greater than the lifetime of the Universe $\tau_U \sim 10^{17}$ sec [89], and in such a case, we say that the EW vacuum is metastable. The decay probability of the EW vacuum to the true vacuum at the present epoch has been computed using the bounce solution of the Euclidean equations of motion of the Higgs field [35,90,91],

$$\mathcal{P}_0 = 0.15\frac{\Lambda_B^4}{H^4}e^{-S(\Lambda_B)}, \quad \text{where } S(\Lambda_B) = \frac{8\pi^2}{3|\lambda_{\rm eff}(\Lambda_B)|}.$$
(5.4)

Here, H is the Hubble constant, and $S(\Lambda_B)$ is the minimum action of the Higgs potential at the bounce size $R = \Lambda_B^{-1}$, which gives the dominant contribution to the tunneling probability $\mathcal{P}_0$. The metastable EW vacuum implies that the decay probability $\mathcal{P}_0 < 1$. This can be translated into a bound on the Higgs effective quartic coupling $\lambda_{\rm eff}$, which can be read as [79,91,92]

$$\lambda_{\rm eff} > \lambda_{\rm eff\,min}(\Lambda_B) = \frac{-0.06488}{1 - 0.00986\ln{(v/\Lambda_B)}}.$$
(5.5)

$\lambda_{\rm eff}(\Lambda_B) < \lambda_{\rm eff\,min}(\Lambda_B)$ corresponds to the unstable region, and the EW vacuum is absolutely stable at $\lambda_{\rm eff}(\Lambda_B) > 0$. Also, the theory violates the perturbative unitarity at $\lambda_{\rm eff}(\Lambda_B) > \frac{4\pi}{3}$ [93].

In Fig. 3, we show the running of the Higgs quartic coupling for four different sets of benchmark points for the minimal type-III seesaw model. In the left plot, the purple and gray lines correspond to $M_t = 171.3$ and 174.9 GeV,
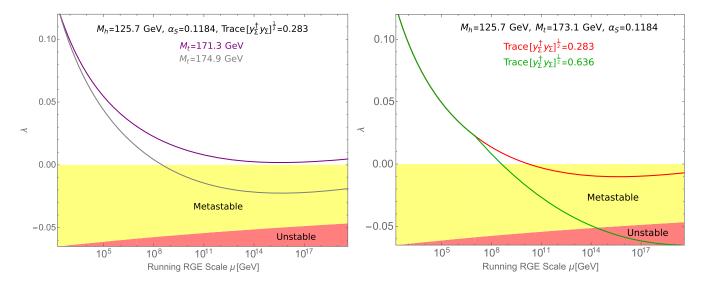
FIG. 3.   RG evolution of the Higgs quartic coupling. The plot on the left side shows the running of λ for different values of M_t with fixed M_Σ and $\mathrm{Tr}[Y_\Sigma^\dagger Y_\Sigma]^{\frac{1}{2}}$, whereas the plot on the right side shows the running of λ for different values of $\mathrm{Tr}[Y_\Sigma^\dagger Y_\Sigma]^{\frac{1}{2}}$ with M_Σ and M_t fixed. For both plots, we have taken $M_{\Sigma 1} = M_{\Sigma 2} = M_\Sigma = 10^7$ GeV.

respectively, with the value of $\mathrm{Tr}[Y_\Sigma^\dagger Y_\Sigma]^{\frac{1}{2}}$ fixed as 0.283 and $M_\Sigma = 10^7$ GeV. For the first case, we can see that the Higgs quartic coupling λ remains positive up to the Planck scale; i.e., the EW vacuum is absolutely stable up to the M_{Pl}. For $M_t = 174.9$ GeV, we can see that $\lambda \sim \lambda_{\mathrm{eff}}$ becomes negative at the energy scale $\sim 10^9$ GeV, the so-called instability scale Λ_I, and remains negative up to M_{Pl}. However, we find that the beta function of the Higgs quartic coupling $\beta_\lambda(\equiv dV(h)/dh)$ becomes zero around the energy scale $\sim 10^{17}$ GeV, which implies that there is an extra deeper minima at that scale, and we have checked that the EW vacuum corresponding to this point is metastable. Similarly, in the right plot, we have given the running of the quartic coupling for two different values of $\mathrm{Tr}[Y_\Sigma^\dagger Y_\Sigma]^{\frac{1}{2}}$ with fixed M_t and M_Σ. We notice that as the value of the $\mathrm{Tr}[Y_\Sigma^\dagger Y_\Sigma]$ is increased from 0.283 to 0.636, the EW vacuum shifts from the metastable to the unstable region. In this way, the conditions of stability and metastability can put constraints on the allowed values of $\mathrm{Tr}[Y_\Sigma^\dagger Y_\Sigma]^{\frac{1}{2}}$.

A. Phase diagram of vacuum stability

As we have already discussed, the present central values of the SM parameters imply that an extra deeper minima exists near the Planck scale. Hence, there is a possibility that the EW vacuum might tunnel into that true (deeper) vacuum. In the type-III seesaw model, depending upon the new physics parameter space, the stability of the EW vacuum is modified compared to that in the SM, and there are two effects contributing to this. The first one is the negative contribution to the running of λ as well as to the effective Higgs potential due to the triplet fermion Yukawa coupling [see Eqs. (5.3) and (A1)]. The second one

is through the modified RGE for the $SU(2)$ gauge coupling g_2 [Eq. (A3)], which in turn gives a positive contribution to the running of λ. These effects have also been discussed in Ref. [45].

In Fig. 4, we have given the phase diagram in the $\mathrm{Tr}[Y_\Sigma^\dagger Y_\Sigma]^{\frac{1}{2}} - M_\Sigma$ plane for the central values of the SM parameters $M_t = 173.1$, $M_h = 125.7$, and $\alpha_s = 0.1184$. Here, the horizontal red solid line separating the unstable region (red) and the metastable (yellow) region is obtained when $\beta_\lambda(\mu) = 0$ along with $\lambda(\mu) = \lambda_{\min}(\Lambda_B)$. From this plot, we can see that the parameter space with $\mathrm{Tr}[Y_\Sigma^\dagger Y_\Sigma]^{\frac{1}{2}} \gtrsim 0.64$
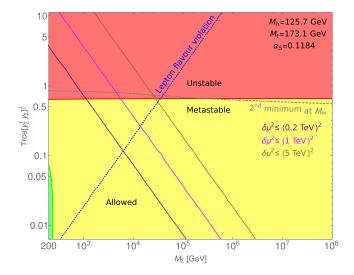

FIG. 4.   The phase diagram in the $\mathrm{Tr}[Y_\Sigma^\dagger Y_\Sigma]^{\frac{1}{2}}$-$M_\Sigma$ plane for NH. Here, we have used the central values of M_t, M_h, and α_s. The color coding of the lines (blue, purple, magenta, and brown) is the same as in Fig. 2. The horizontal red solid line separates the unstable and the metastable regions of the EW vacuum.

FIG. 5. The phase diagram in the $\mathrm{Tr}[Y_\Sigma^\dagger Y_\Sigma]^{\frac{1}{2}}$-$M_\Sigma$ plane for NH. The plot on the left (right) side gives the most liberal (stringent) bound from vacuum stability with minimum (maximum) value of M_t and maximum (minimum) values of M_h and α_s. The color coding of the lines (blue, purple, magenta, and brown) is the same as in Fig. 2. The horizontal red solid line separates the unstable and the metastable regions of the EW vacuum.
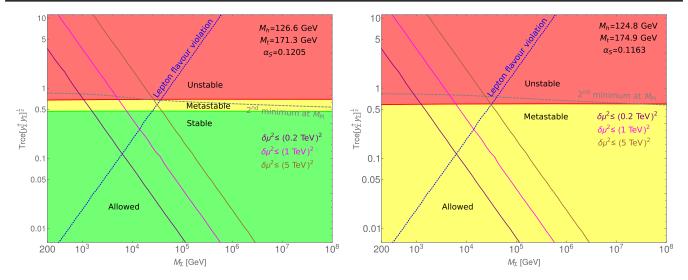
with the heavy fermion mass scale 200–10^8 GeV is excluded by instability of the EW vacuum. The gray dashed line corresponds to the points for which the beta function of the quartic coupling λ is zero at the Planck scale; i.e., the second minima is situated at that scale. Also, we can see a very small green region for the lower values of masses and couplings for which the EW vacuum is absolutely stable. However, this region is disfavored from the LFV constraints as shown by the blue dotted line. The region to the right of this line is allowed by the current bounds from LFV as given in Eq. (4.2). We have also given the bounds from naturalness in these figures as shown by the slanted solid lines corresponding to three different values of $\delta\mu^2$. Thus, one can see that the area that is allowed both by naturalness as well as LFV falls in the stability/metastability region.

In Fig. 5, we have again plotted the phase diagram in the $\mathrm{Tr}[Y_\Sigma^\dagger Y_\Sigma]^{\frac{1}{2}}$-$M_\Sigma$ plane for the NH, but with different values of SM parameters. The panel on the left (right) side gives the most liberal (stringent) bound from vacuum stability with minimum (maximum) value of M_t and maximum (minimum) values of M_h and α_s from their allowed 3σ ranges. Clearly, with the smallest value of M_t and the largest values of M_h and α_s, the stability region increases, as is shown by the green region in the panel on the left-hand side. On the other hand, in the right panel with the highest value of M_t and lowest values of M_h and α_s, no region of stability is found. In this case, the parameter space with $\mathrm{Tr}[Y_\Sigma^\dagger Y_\Sigma]^{\frac{1}{2}} > 0.68 \ (0.58)$ is disfavored from the instability condition in the left (right) panels.

Figure 6 gives the phase diagram in the M_t-$\mathrm{Tr}[Y_\Sigma^\dagger Y_\Sigma]^{\frac{1}{2}}$ plane for the NH with the central values of M_h and α_s. The dashed lines separate the metastable and the unstable

regions, whereas the solid lines separate the stable and the metastable regions. The red, blue, and purple colored lines correspond to the representative values of M_Σ as 10^4, 10^7, and 10^{12} GeV, respectively. The two vertical lines give the LFV and the naturalness ($\delta\mu^2 < 1$ TeV^2) bounds for
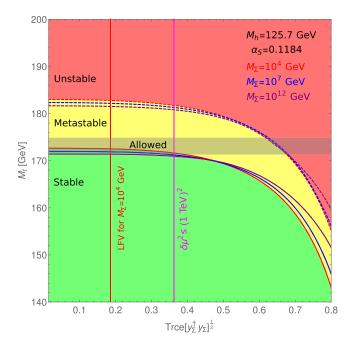

FIG. 6. The phase diagram in the M_t-$\mathrm{Tr}[Y_\Sigma^\dagger Y_\Sigma]^{\frac{1}{2}}$ plane for the NH for the central values of M_h and α_s. The dashed lines separate the metastable and the unstable regions, whereas the solid lines separate the stable and the metastable regions. The three colors are for three different values of M_Σ. The two vertical lines give the LFV and naturalness bounds for $M_\Sigma = 10^4$ GeV, and the region on the left of the LFV line (red) is allowed by both.
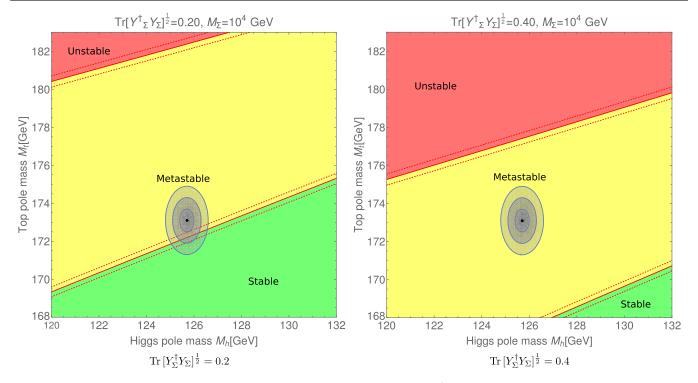
FIG. 7.   The phase diagram in the M_t-M_h plane for two different values of $\mathrm{Tr}[Y_\Sigma^\dagger Y_\Sigma]^{\frac{1}{2}}$ and $M_\Sigma = 10^4$ GeV. The ellipses correspond to the allowed values of M_t and M_h at 1σ, 2σ, and 3σ.

$M_\Sigma = 10^4$ GeV, and the allowed region is to the left of the red vertical line. The horizontal shaded gray region denotes the 3σ allowed range of M_t. It is seen that in this region, the vacuum is metastable for lower values of $\mathrm{Tr}[Y_\Sigma^\dagger Y_\Sigma]^{\frac{1}{2}}$, while for higher values, the vacuum is unstable. Once we consider the bounds from LFV, $\mathrm{Tr}[Y_\Sigma^\dagger Y_\Sigma]^{\frac{1}{2}}$ is less than 0.18 and the vacuum is in the metastable region.

In Fig. 7, we have shown the phase diagram in the M_t-M_h plane for $M_\Sigma = 10^4$ GeV. The red dashed lines correspond to the 3σ variation in α_s. The figures on the left- and right-hand sides correspond to $\mathrm{Tr}[Y_\Sigma^\dagger Y_\Sigma]^{\frac{1}{2}} = 0.20$ and 0.40, respectively. The ellipses correspond to the allowed values of M_t and M_h at 1σ, 2σ, and 3σ. From this figure, we can clearly see that higher values of M_t and Y_Σ affect the stability of the EW vacuum negatively, whereas a higher value of M_h has a positive effect on the stability. For $\mathrm{Tr}[Y_\Sigma^\dagger Y_\Sigma]^{\frac{1}{2}} = 0.20$, some areas of the parameter space fall in the stable region when M_t and M_h are taken in the 3σ ranges, whereas for $\mathrm{Tr}[Y_\Sigma^\dagger Y_\Sigma]^{\frac{1}{2}} = 0.40$, all the allowed parameter space is in the metastable region.

It is also important to look at the change in the confidence level at which the (meta)stability is excluded or allowed [79,92,94] in the context of the minimal type-III seesaw model. The confidence level plot(s) will provide a quantitative measurement of the (meta)stability for the new physics parameter space. In Fig. 8, we show how the confidence level at which EW vacuum is allowed (excluded) from the

metastability (instability) depends on new Yukawa couplings of the heavy fermions for the type-III seesaw model for different values of M_Σ and α_s. To plot these, we have considered the variation of M_t (from 160 to 180 GeV) and M_h (from 120 to 132 GeV) in the $M_t - M_h$ plane for fixed values of α_s. We draw the metastability line and an ellipse to which the metastability line is the tangent and the point corresponding to the central values of M_t and M_h ($M_t = 173.1$ GeV, $M_h = 125.7$ GeV) as the center (see Fig. 7, for instance). Then we calculate the confidence level as confidence level $= \frac{a \text{ of the ellipse}}{1\sigma \text{ error of } M_t} = \frac{b \text{ of the ellipse}}{1\sigma \text{ error of } M_h}$, where a and b are the lengths of the major and minor axes of the ellipse. Figures 8(a) and 8(b) are plotted with the triplet masses as $M_\Sigma = 10^4$ and 10^{12} GeV, respectively. In both cases, the EW vacuum is metastable for smaller values of the new Yukawa coupling. We can see that the confidence level at which the EW vacuum is metastable (yellow region) increases with the increase of $\mathrm{Tr}[Y_\Sigma^\dagger Y_\Sigma]^{\frac{1}{2}}$. Also, one can see that the confidence level at which the EW vacuum is metastable increases with the increase in the mass of the fermion triplets. We can also see the effect of α_s on the confidence level. The dashed, solid, and dotted red lines correspond to the values of α_s as 0.1177, 0.1184, and 0.1191, respectively. Clearly, the confidence level at which the EW vacuum is metastable decreases with the increase in α_s. This is because α_s has a positive effect on the stability of the EW vacuum, and the increase in α_s increases the confidence level at which the vacuum is stable, thereby decreasing the
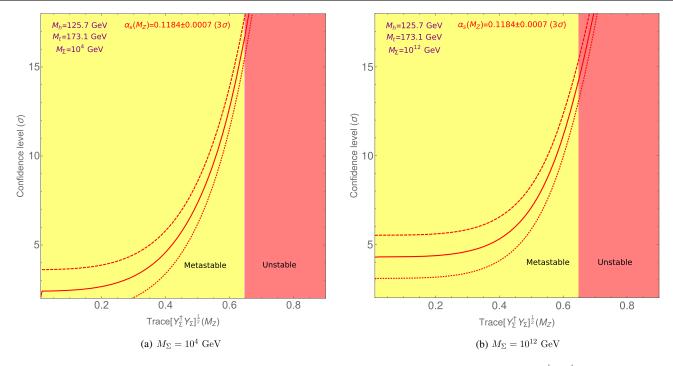
(a) $M_\Sigma = 10^4$ GeV

(b) $M_\Sigma = 10^{12}$ GeV

FIG. 8. Dependence of confidence level at which the EW vacuum stability is excluded/allowed on $\mathrm{Tr}[Y_\Sigma^\dagger Y_\Sigma]^{\frac{1}{2}}$ for different values of α_s and M_Σ.

confidence level at which it is unstable. The EW vacuum becomes metastable for $\mathrm{Tr}[Y_\Sigma^\dagger Y_\Sigma]^{\frac{1}{2}} = 0.646 \pm 0.008$ and $\mathrm{Tr}[Y_\Sigma^\dagger Y_\Sigma]^{\frac{1}{2}} = 0.648 \pm 0.011$ corresponding to $\alpha_s = 0.1184 \pm 0.0007$ for $M_\Sigma = 10^4$ and 10^{12} GeV, respectively. The demarcations between the stable and the metastable regions in the plots are only for the central values of α_s.

VI. SUMMARY

In this paper, we have analyzed the implications of naturalness and the stability of the electroweak vacuum in the context of the minimal type-III seesaw model. We have also studied the constraints from lepton flavor violating decays. We have found that the lighter masses of the fermionic triplets $M_\Sigma \simeq 400$ GeV are disallowed for all values of Y_Σ by the constraints from the $\mu \to e$ conversion in the nucleus. At the same time, the heavier triplet masses are disfavored by naturalness. For instance, if we demand the correction to the Higgs mass to be less than 200 GeV, it will put an upper bound of $\sim 10^5$ GeV on the masses of the triplets. Also, the maximum value of $\mathrm{Tr}[Y_\Sigma^\dagger Y_\Sigma]^{\frac{1}{2}}$ that is allowed is 0.1, corresponding to $M_\Sigma \sim 10^4$ GeV. Another important result is that in the parameter space which is allowed by both the LFV as well as naturalness constraints, the EW vacuum is stable/metastable depending on the values of $\mathrm{Tr}[Y_\Sigma^\dagger Y_\Sigma]^{\frac{1}{2}}$ and the standard model parameters used. Hence, one does not really have to worry about the instability of the vacuum in this model. The major part of the allowed parameter space lies in a region that could be tested in the future collider experiments.

APPENDIX: RENORMALIZATION GROUP EQUATIONS

The beta functions for the various couplings are defined as

$$\beta_{\chi_i} = \frac{\partial \chi_i}{\partial \ln \mu} = \frac{1}{16\pi^2} \beta_{\chi_i}^{(1)} + \frac{1}{(16\pi^2)^2} \beta_{\chi_i}^{(2)}.$$

For the running scale $\mu < M_\Sigma$,

$$\beta_{\chi_i} = \beta_{\chi_i}^{\mathrm{SM}}, \qquad \beta_{g_2}^{(1)} = -\frac{19}{6} g_2^3, \quad \text{and} \quad \beta_{Y_\Sigma} = 0,$$

and for $\mu > M_\Sigma$, the one-loop RGEs for λ, y_t, g_2, and Y_Σ are as given below

$$\beta_\lambda = \frac{3}{8} g_1^4 + \frac{3}{4} g_1^2 g_2^2 + \frac{9}{8} g_2^4 - 3 g_1^2 \lambda - 9 g_2^2 \lambda + 24\lambda^2 + 12\lambda y_t^2 - 6 y_t^4 + 12\lambda \mathrm{Tr}(Y_\Sigma Y_\Sigma^\dagger) - 10 \mathrm{Tr}(Y_\Sigma Y_\Sigma^\dagger Y_\Sigma Y_\Sigma^\dagger), \qquad (A1)$$

$$\beta_{y_t} = y_t \left(\frac{9}{2} y_t^2 - 8 g_3^2 - \frac{17}{12} g_1^2 - \frac{9}{4} g_2^2 + 3 \mathrm{Tr}(Y_\Sigma Y_\Sigma^\dagger) \right), \qquad (A2)$$

$$\beta_{g_2} = -\frac{1}{2}g_2^3, \tag{A3}$$

$$\beta_{Y_\Sigma} = Y_\Sigma \left(\frac{5}{2} Y_\Sigma Y_\Sigma^\dagger + 3y_t^2 - \frac{33}{4}g_2^2 - \frac{3}{4}g_1^2 + 3\mathrm{Tr}(Y_\Sigma Y_\Sigma^\dagger) \right). \tag{A4}$$

Two-loop RGEs used in this work have been generated using SARAH [95]. In our work, we have taken only the top-quark contributions. The other SM-Yukawa couplings are comparatively smaller, and their inclusion does not alter our result.

[1] S. Chatrchyan *et al.* (CMS Collaboration), Observation of a new boson at a mass of 125 GeV with the CMS experiment at the LHC, Phys. Lett. B **716,** 30 (2012).

[2] G. Aad *et al.* (ATLAS Collaboration), Observation of a new particle in the search for the Standard Model Higgs boson with the ATLAS detector at the LHC, Phys. Lett. B **716,** 1 (2012).

[3] S. Weinberg, Baryon- and Lepton-Nonconserving Processes, Phys. Rev. Lett. **43,** 1566 (1979).

[4] P. Minkowski, $\mu \to e\gamma$ at a rate of one out of 10^9 muon decays, Phys. Lett. B **67,** 421 (1977).

[5] M. Gell-Mann, P. Ramond, and R. Slansky, in *Proceedings of the Supergravity Workshop*, 1979, p. 315.

[6] T. Yanagida, in *Proceedings of the Workshop on Unified Theory and Baryon Number in the Universe*, 1979, p. 95.

[7] R. N. Mohapatra and G. Senjanovic, Neutrino Mass and Spontaneous Parity Violation, Phys. Rev. Lett. **44,** 912 (1980).

[8] J. Schechter and J. Valle, Neutrino masses in $\mathrm{SU}(2) \times \mathrm{U}(1)$ theories, Phys. Rev. D **22,** 2227 (1980).

[9] J. Schechter and J. Valle, Neutrino decay and spontaneous violation of lepton number, Phys. Rev. D **25,** 774 (1982).

[10] G. Lazarides, Q. Shafi, and C. Wetterich, Proton lifetime and fermion masses in an SO(10) model, Nucl. Phys. **B181,** 287 (1981).

[11] R. N. Mohapatra and G. Senjanovic, Neutrino masses and mixings in gauge models with spontaneous parity violation, Phys. Rev. D **23,** 165 (1981).

[12] R. Foot, H. Lew, X. He, and G. C. Joshi, Seesaw neutrino masses induced by a triplet of leptons, Z. Phys. C **44,** 441 (1989).

[13] R. Mohapatra and J. Valle, Neutrino mass and baryon number nonconservation in superstring models, Phys. Rev. D **34,** 1642 (1986).

[14] P.-H. Gu and U. Sarkar, Leptogenesis with linear, inverse or double seesaw, Phys. Lett. B **694,** 226 (2010).

[15] H. Zhang and S. Zhou, The minimal seesaw model at the TeV scale, Phys. Lett. B **685,** 297 (2010).

[16] M. Hirsch, S. Morisi, and J. Valle, A4-based tri-bimaximal mixing within inverse and linear seesaw schemes, Phys. Lett. B **679,** 454 (2009).

[17] M. Gavela, T. Hambye, D. Hernandez, and P. Hernandez, Minimal flavour seesaw models, J. High Energy Phys. 09 (2009) 038.

[18] S. M. Boucenna, S. Morisi, and J. W. F. Valle, The low-scale approach to neutrino masses, Adv. High Energy Phys. **2014,** 1 (2014).

[19] F. F. Deppisch, P. S. Bhupal Dev, and A. Pilaftsis, Neutrinos and collider physics, New J. Phys. **17,** 075019 (2015).

[20] R. Adhikari and A. Raychaudhuri, Light neutrinos from massless texture and below TeV seesaw scale, Phys. Rev. D **84,** 033002 (2011).

[21] J. Kersten and A. Y. Smirnov, Right-handed neutrinos at CERN LHC and the mechanism of neutrino mass generation, Phys. Rev. D **76,** 073005 (2007).

[22] A. Pilaftsis, Radiatively induced neutrino masses and large Higgs neutrino couplings in the standard model with Majorana fields, Z. Phys. C **55,** 275 (1992).

[23] F. Vissani, Do experiments suggest a hierarchy problem?, Phys. Rev. D **57,** 7027 (1998).

[24] J. A. Casas, J. R. Espinosa, and I. Hidalgo, Implications for new physics from fine-tuning arguments. 1. Application to SUSY and seesaw cases, J. High Energy Phys. 11 (2004) 057.

[25] A. Abada, C. Biggio, F. Bonnet, M. Gavela, and T. Hambye, Low energy effects of neutrino masses, J. High Energy Phys. 12 (2007) 061.

[26] M. Farina, D. Pappadopulo, and A. Strumia, A modified naturalness principle and its experimental tests, J. High Energy Phys. 08 (2013) 022.

[27] J. D. Clarke, R. Foot, and R. R. Volkas, Electroweak naturalness in the three-flavor type I seesaw model and implications for leptogenesis, Phys. Rev. D **91,** 073009 (2015).

[28] M. Fabbrichesi and A. Urbano, Naturalness redux: The case of the neutrino seesaw mechanism, Phys. Rev. D **92,** 015028 (2015).

[29] J. D. Clarke, R. Foot, and R. R. Volkas, Natural leptogenesis and neutrino masses with two Higgs doublets, Phys. Rev. D **92,** 033006 (2015).

[30] M. Chabab, M. C. Peyranre, and L. Rahili, Naturalness in a type II seesaw model and implications for physical scalars, Phys. Rev. D **93,** 115021 (2016).

[31] N. Haba, H. Ishida, N. Okada, and Y. Yamaguchi, Vacuum stability and naturalness in type-II seesaw, Eur. Phys. J. C **76,** 333 (2016).

[32] G. Bambhaniya, P. S. Bhupal Dev, S. Goswami, S. Khan, and W. Rodejohann, Naturalness, vacuum stability and leptogenesis in the minimal seesaw model, Phys. Rev. D **95,** 095016 (2017).

[33] P. S. B. Dev, C. M. Vila, and W. Rodejohann, Naturalness in testable type II seesaw scenarios, Nucl. Phys. **B921**, 436 (2017).

[34] S. Alekhin, A. Djouadi, and S. Moch, The top quark and Higgs boson masses and the stability of the electroweak vacuum, Phys. Lett. B **716**, 214 (2012).

[35] D. Buttazzo, G. Degrassi, P. P. Giardino, G. F. Giudice, F. Sala, A. Salvio, and A. Strumia, Investigating the near-criticality of the Higgs boson, J. High Energy Phys. 12 (2013) 089.

[36] W. Rodejohann and H. Zhang, Impact of massive neutrinos on the Higgs self-coupling and electroweak vacuum stability, J. High Energy Phys. 06 (2012) 022.

[37] J. Chakrabortty, M. Das, and S. Mohanty, Constraints on TeV scale Majorana neutrino phenomenology from the vacuum stability of the Higgs, Mod. Phys. Lett. A **28**, 1350032 (2013).

[38] S. Khan, S. Goswami, and S. Roy, Vacuum Stability constraints on the minimal singlet TeV seesaw model, Phys. Rev. D **89**, 073021 (2014).

[39] A. Datta, A. Elsayed, S. Khalil, and A. Moursy, Higgs vacuum stability in the $B - L$ extended standard model, Phys. Rev. D **88**, 053011 (2013).

[40] J. Chakrabortty, P. Konar, and T. Mondal, Constraining a class of $B - L$ extended models from vacuum stability and perturbativity, Phys. Rev. D **89**, 056014 (2014).

[41] A. Kobakhidze and A. Spencer-Smith, Neutrino masses and Higgs vacuum stability, J. High Energy Phys. 08 (2013) 036.

[42] J. N. Ng and A. de la Puente, Electroweak vacuum stability and the seesaw mechanism revisited, Eur. Phys. J. C **76**, 122 (2016).

[43] L. D. Rose, C. Marzo, and A. J. Urbano, On the stability of the electroweak vacuum in the presence of low-scale seesaw models, J. High Energy Phys. 12 (2015) 050.

[44] G. Bambhaniya, S. Khan, P. Konar, and T. Mondal, Constraints on a seesaw model leading to quasidegenerate neutrinos and signatures at the LHC, Phys. Rev. D **91**, 095007 (2015).

[45] M. Lindner, H. H. Patel, and B. Radovi, Electroweak absolute, meta-, and thermal stability in neutrino mass models, Phys. Rev. D **93**, 073005 (2016).

[46] A. Das, N. Okada, and N. Papapietro, Electroweak vacuum stability in classically conformal B-L extension of the Standard Model, Eur. Phys. J. C **77**, 122 (2017).

[47] A. Das, S. Oda, N. Okada, and D.-s. Takahashi, Classically conformal U(1) extended standard model, electroweak vacuum stability, and LHC Run-2 bounds, Phys. Rev. D **93**, 115038 (2016).

[48] S. Bhattacharya, P. Ghosh, T. N. Maity, and T. S. Ray, Mitigating direct detection bounds in non-minimal Higgs portal scalar dark matter models, J. High Energy Phys. 10 (2017) 088.

[49] I. Garg, S. Goswami, V. K. N., and N. Khan, Electroweak vacuum stability in presence of singlet scalar dark matter in TeV scale seesaw models, Phys. Rev. D **96**, 055020 (2017).

[50] B. He, N. Okada, and Q. Shafi, 125 GeV Higgs, type III seesaw and gauge Higgs unification, Phys. Lett. B **716**, 197 (2012).

[51] J. Casas and A. Ibarra, Oscillating neutrinos and $\mu \to e, \gamma$, Nucl. Phys. **B618**, 171 (2001).

[52] A. Ibarra and G. G. Ross, Neutrino phenomenology: The case of two right-handed neutrinos, Phys. Lett. B **591**, 285 (2004).

[53] W. Grimus and L. Lavoura, The seesaw mechanism at arbitrary order: Disentangling the small scale from the large scale, J. High Energy Phys. 11 (2000) 042.

[54] I. Esteban, M. C. Gonzalez-Garcia, M. Maltoni, I. Martinez-Soler, and T. Schwetz, Updated fit to three neutrino mixing: Exploring the accelerator-reactor complementarity, J. High Energy Phys. 01 (2017) 087.

[55] A. Abada, C. Biggio, F. Bonnet, M. B. Gavela, and T. Hambye, $\mu \to e\gamma$ and $\tau \to l\gamma$ decays in the fermion triplet seesaw model, Phys. Rev. D **78**, 033007 (2008).

[56] B. Bajc and G. Senjanovic, Seesaw at LHC, J. High Energy Phys. 08 (2007) 014.

[57] B. Bajc, M. Nemevsek, and G. Senjanovic, Probing seesaw at LHC, Phys. Rev. D **76**, 055011 (2007).

[58] R. Franceschini, T. Hambye, and A. Strumia, Type-III seesaw at LHC, Phys. Rev. D **78**, 033002 (2008).

[59] F. del Aguila and J. Aguilar-Saavedra, Distinguishing seesaw models at LHC with multi-lepton signals, Nucl. Phys. **B813**, 22 (2009).

[60] T. Li and X.-G. He, Neutrino masses and heavy triplet leptons at the LHC: Testability of type III seesaw, Phys. Rev. D **80**, 093003 (2009).

[61] P. Bandyopadhyay, S. Choi, E. J. Chun, and K. Min, Probing Higgs bosons via the type III seesaw mechanism at the LHC, Phys. Rev. D **85**, 073013 (2012).

[62] O. J. P. Eboli, J. Gonzalez-Fraile, and M. C. Gonzalez-Garcia, Neutrino masses at LHC: Minimal lepton flavour violation in type-III see-saw, J. High Energy Phys. 12 (2011) 009.

[63] F. von der Pahlen, G. Palacio, D. Restrepo, and O. Zapata, Radiative type III seesaw model and its collider phenomenology, Phys. Rev. D **94**, 033005 (2016).

[64] R. Ruiz, QCD corrections to pair production of type III seesaw leptons at hadron colliders, J. High Energy Phys. 12 (2015) 1.

[65] CMS Collaboration, Search for Evidence of the Type-III Seesaw Mechanism in Multilepton Final States in Proton-Proton Collisions at $\sqrt{s} = 13$ TeV, Phys. Rev. Lett. **119**, 221802 (2017).

[66] G. Aad *et al.* (ATLAS Collaboration), Search for type-III seesaw heavy leptons in pp collisions at $\sqrt{s} = 8$ TeV with the ATLAS detector, Phys. Rev. D **92**, 032001 (2015).

[67] D. Goswami and P. Poulose, Direct searches of type III seesaw triplet fermions at high energy e^+e^- collider, Eur. Phys. J. C **78**, 42 (2018).

[68] C. Dohmen *et al.* (SINDRUM II Collaboration), Test of lepton flavor conservation in $\mu \to e$ conversion on titanium, Phys. Lett. B **317**, 631 (1993).

[69] J. Casas, J. Espinosa, and M. Quiros, Improved Higgs mass stability bound in the standard model and implications for supersymmetry, Phys. Lett. B **342**, 171 (1995).

[70] G. Altarelli and G. Isidori, Lower limit on the Higgs mass in the standard model: An update, Phys. Lett. B **337**, 141 (1994).

[71] J. A. Casas, J. R. Espinosa, M. Quiros, and A. Riotto, The lightest Higgs boson mass in the minimal supersymmetric

standard model, Nucl. Phys. **B436**, 3 (1995); Erratum, Nucl. Phys.**B439**, 466(E) (1995).

[72] J. Casas, J. Espinosa, and M. Quiros, Standard model stability bounds for new physics within LHC reach, Phys. Lett. B **382**, 374 (1996).

[73] M. Quiros, Constraints on the Higgs boson properties from the effective potential, arXiv:hep-ph/9703412.

[74] J. A. Casas, V. Di Clemente, A. Ibarra, and M. Quiros, Massive neutrinos and the Higgs mass window, Phys. Rev. D **62**, 053005 (2000).

[75] C. Ford, D. Jones, P. Stephenson, and M. Einhorn, The effective potential and the renormalization group, Nucl. Phys. **B395**, 17 (1993).

[76] A. Sirlin and R. Zucchini, Dependence of the quartic coupling H(m) on M(H) and the possible onset of new physics in the Higgs sector of the standard model, Nucl. Phys. **B266**, 389 (1986).

[77] F. Bezrukov, M. Y. Kalmykov, B. A. Kniehl, and M. Shaposhnikov, Higgs boson mass and new physics, J. High Energy Phys. 10 (2012) 140.

[78] G. Degrassi, S. Di Vita, J. Elias-Miro, J. R. Espinosa, G. F. Giudice, G. Isidori, and A. Strumia, Higgs mass and vacuum stability in the standard model at NNLO, J. High Energy Phys. 08 (2012) 098.

[79] N. Khan and S. Rakshit, Study of electroweak vacuum metastability with a singlet scalar dark matter, Phys. Rev. D **90**, 113008 (2014).

[80] K. Melnikov and T. v. Ritbergen, The three loop relation between the MS-bar and the pole quark masses, Phys. Lett. B **482**, 99 (2000).

[81] R. Hempfling and B. A. Kniehl, On the relation between the fermion pole mass and MS Yukawa coupling in the standard model, Phys. Rev. D **51**, 1386 (1995).

[82] B. Schrempp and M. Wimmer, Top quark and Higgs boson masses: Interplay between infrared and ultraviolet physics, Prog. Part. Nucl. Phys. **37**, 1 (1996).

[83] F. Jegerlehner and M. Y. Kalmykov, $O(\alpha\alpha_s)$ correction to the pole mass of the t-quark within the standard model, Nucl. Phys. **B676**, 365 (2004).

[84] K. Chetyrkin and M. Zoller, Three-loop β-functions for top-Yukawa and the Higgs self-interaction in the standard model, J. High Energy Phys. 06 (2012) 033.

[85] M. F. Zoller, Vacuum stability in the SM and the three-loop β-function for the Higgs self-interaction, Subnuclear series **50**, 557 (2014).

[86] K. G. Chetyrkin and M. F. Zoller, β-function for the Higgs self-interaction in the standard model at three-loop level, J. High Energy Phys. 04 (2013) 091; Erratum, J. High Energy Phys.09 (2013) 155(E).

[87] M. Zoller, Beta-function for the Higgs self-interaction in the standard model at three-loop level, Proc. Sci., EPS-HEP2013 (**2013**) 322.

[88] J. Chakrabortty, A. Dighe, S. Goswami, and S. Ray, Renormalization group evolution of neutrino masses and mixing in the type-III seesaw mechanism, Nucl. Phys. **B820**, 116 (2009).

[89] P. A. R. Ade *et al.* (Planck Collaboration), Planck 2015 results. XIII. Cosmological parameters, Astron. Astrophys. **594**, A13 (2016).

[90] S. R. Coleman, The fate of the false vacuum. 1. Semi-classical theory, Phys. Rev. D **15**, 2929 (1977).

[91] G. Isidori, G. Ridolfi, and A. Strumia, On the metastability of the standard model vacuum, Nucl. Phys. **B609**, 387 (2001).

[92] N. Khan and S. Rakshit, Constraints on inert dark matter from the metastability of the electroweak vacuum, Phys. Rev. D **92**, 055006 (2015).

[93] B. W. Lee, C. Quigg, and H. B. Thacker, Weak interactions at very high-energies: The role of the Higgs boson mass, Phys. Rev. D **16**, 1519 (1977).

[94] N. Khan, Exploring hyperchargeless Higgs triplet model up to the Planck scale, Eur. Phys. J. C **78**, 341 (2018).

[95] F. Staub, SARAH 4: A tool for (not only SUSY) model builders, Comput. Phys. Commun. **185**, 1773 (2014).